DOI: https://doi.org/10.15276/hait.09.2026.33
UDC 004.92

Modified neural models based on the bidirectional reflectance distribution functions

Oleksandr N. Romanyuk[1)]
ORCID: https://orcid.org/0000-0002-2245-3364; rom8591@gmail.com. Scopus Author ID: 57105210600
Yevhen K. Zavalniuk[1)]
ORCID: https://orcid.org/0009-0005-1202-4653; qq9272627@gmail.com. Scopus Author ID: 58643724500
Ruslan P. Shevchuk[2)]
ORCID: https://orcid.org/0000-0001-5381-9528; rulezz.sh@gmail.com. Scopus Author ID: 24178081800
Oleksandr A. Siropiatov[3)]
ORCID: https://orcid.org/0000-0002-6362-1280; o.a.syropiatov@op.edu.ua
[1)] Vinnytsia National Technical University, 95, Khmelnytske Highway Str. Vinnytsia, 21021, Ukraine
[2)] University of Bielsko-Biała, 2, Willowa Str. Bielsko-Biała, 43-300, Poland
[3)] Odesa Polytechnic National University, 1, Shevchenko Ave. Odesa, 65044, Ukraine

ABSTRACT

Bidirectional reflectance distribution functions are used to model light reflection from object surfaces. Empirical and microfacet analytical bidirectional reflectance distribution functions are most often used, but they do not always provide sufficiently accurate reproduction of reflection features. Tables of measured values provide highly realistic representation of material reflective properties but require significant computational resources. Therefore, neural bidirectional reflectance distribution functions **are relevant** for dense representation of measured values. The study is **aimed** at developing modified neural models for more efficient and accurate modeling of light reflection. Machine learning and computer modeling **research methods** were used. **The results of the study** include the usage of physically meaningful material features together with a single block of weight parameters for compact representation of a fixed material set. It provides accurate reflectance value prediction without additional computational units or recalculation of material features. Neural bidirectional reflectance distribution functions based on material clusters are also proposed, enabling the use of a relatively small number of neural network weight files and minimal material features, thereby increasing reflectance values prediction performance. A combined process of material cluster formation is described. The adaptive combining of transformation functions for high-dynamic-range of reflectance values at the stage of neural network training is considered. Improved prediction accuracy for new test materials is demonstrated. The proposed models are implemented in the 3D-rendering tool Idx3d. In **conclusion**, the developed models enable the use of a single set of weight parameters, more productive reflectance prediction, and more efficient processing of training values.

Keywords: Computer graphics; rendering; software engineering; neural network; neural rendering; bidirectional reflectance distribution function

***For citation*: Romanyuk O. N., Zavalniuk Y. K., Shevchuk R. P. Siropiatov O. A. "Modified neural models based on the bidirectional reflectance distribution functions". *Herald of Advanced Information Technology*. 2026; Vol.9 No.4: 521–538. DOI: https://doi.org/10.15276/hait.09.2026.33**

INTRODUCTION

Achieving high realism in image formation is one of the most important tasks in three-dimensional rendering [1], [2]. The level of realism of a 3D-image largely depends on the chosen model of light reflectance from material surfaces. Complex light reflectance models, which consider the roughness of the material surface, its optical features, and the effects of light shadowing and masking, are usually used in the systems of highly realistic rendering. However, analytical reflectance models don't always allow one to fully represent all peculiarities of light reflection from materials. Measurement-based tabular light reflectance models provide a more accurate modeling of light interaction with the surfaces of objects. However, they require a lot of computational resources for storing and accessing the data.

At the same time, the usage of artificial intelligence and machine learning [3], [4], [5], [6], [7] for the tasks of highly realistic 3D-rendering is becoming more common. In particular, neural light reflectance models provide a compact representation of tables of measured material reflectance properties. Moreover, a high rendering speed is achieved. However, existing neural reflectance models are characterized by a number of disadvantages: the use of large number of files with parameters, the use of material features without physical meaning, too high computational complexity, insufficiently effective processing of high-dynamic-range tabular values.

© Romanyuk O., Zavalniuk Y., Shevchuk R., Siropiatov O., 2026

This is an open access article under the CC BY license (https://creativecommons.org/licenses/by/4.0/deed.uk)

In particular, the NBRDF method [8] involves training a neural model for each material, which significantly increases the number of parameter files and total model size. The Hyponet method [9] represents the whole material set using a hypernetwork, but this requires additional computational blocks. In addition, this method uses a single transformation function for high-dynamic-range reflectance values, the effectiveness of which may differ between materials.

Thus, the development of new neural light reflectance models and the modification of existing ones is relevant.

LITERATURE ANALYSIS

During the calculation of the color intensity of a pixel, the ambient lighting (reflected from the external environment) and the reflected light from the surface of the object material are taken into account. Besides, reflected light includes diffuse and specular components. The diffuse light reflection component lies in the reflection of light in different directions and determines the visibility of the object. Specular reflection corresponds to light being reflected in a concentrated direction and determines the formation of a specular highlight at the surface of the object. Diffuse light reflection is more common for matte and rough surfaces, specular reflection – for glossy and metallic surfaces. Bidirectional reflectance distribution functions are usually used for modeling the reflection of light from material surfaces.

The bidirectional reflectance distribution function (BRDF) [10], [11], [12] is a radiometric function that represents the reflective properties of materials and is determined as the ratio of outgoing radiance to incoming irradiance [11]

$$dL_r(\vec{V})/dE_i(\vec{L}), \quad (1)$$

where $L_r(\vec{V})$ is radiance in the direction $\vec{V}$ from the surface point to the observer, $E_i(\vec{L})$ is irradiance in the direction $\vec{L}$ between the light source and surface point.

Fig. 1 shows vectors [13] that are used for BRDF calculation. $\vec{H}$ is a halfvector between $\vec{L}$ and $\vec{V}$, which is calculated using the formula $(\vec{L}+\vec{V})/|\vec{L}+\vec{V}|$, $\vec{R}$ is vector of mirror reflection, which is calculated using the formula $2(\vec{L}\cdot\vec{N})\vec{N}-\vec{L}$, $\vec{N}$ is normal to the surface point. θ_h is angle between $\vec{H}$ and $\vec{N}$, θ_i is angle between $\vec{L}$ and $\vec{N}$, θ_o is angle between $\vec{V}$ and $\vec{N}$, ψ is angle between $\vec{V}$ and $\vec{R}$.

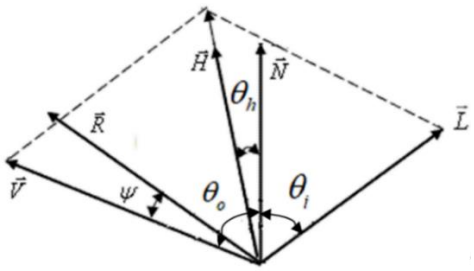


Fig. 1. **Main angles and vectors for BRDF value calculation**
***Source*: compiled by the [13]**

The Lambert BRDF (F_{LMB}) [11] is used for ideally diffuse surfaces, for which the uniform reflection of light in different directions is characteristic. The expression is used

$$F_{LMB} = \frac{\rho_d}{\pi}\cos(\theta_i), \quad (2)$$

where θ_i is angle between $\vec{L}$ and normal to the surface point $\vec{N}$, ρ_d is diffuse albedo.

The BRDF for an ideal specular surface (F_{ISS}) [14] is determined using the delta-function δ

$$F_{ISS} = \rho_s\delta(\vec{L},\vec{V}), \quad (3)$$

where ρ_s is specular albedo. Accordingly, δ has value ∞, when $\vec{R}=\vec{V}$, and value 0 in all other cases. Furthermore, the hemispherical integral reflectance value is 1.

Due to the limited usage area, the ideal specular surface BRDF is relatively rarely used. At the same time, the Lambert BRDF is enough for representing reflectance properties of the majority of diffuse materials. In addition, the function is often used as the idealized diffuse component, which complements the specular BRDF of the real surface.

Empirical BRDFs are simple and are used for the approximate representation of material reflective properties. A well-known function is the empirical Phong BRDF (F_{PH}) [13], [15], [16], which is calculated according to the expression

$$F_{PH} = \cos(\psi)^n, \quad (4)$$

where n is surface shininess coefficient, which determines the degree of concentration of the specular highlight, depending on the reflective properties of the surface material.

The Blinn BRDF [13], [16] ,[17], [18] is an improved Phong BRDF and lies in the calculation of the cosine angle θ_h between $\vec{H}$ and $\vec{N}$ instead of the cosine angle ψ between $\vec{V}$ and $\vec{R}$. Due to their simple form, Phong and Blinn BRDFs are commonly used in the highly productive rendering systems.

ISSN 2663-0176 (Print)
ISSN 2663-7731 (Online)

The detailed aspects of light reflection from the surface materials are not considered in the empirical BRDFs, therefore their usage during the photorealistic rendering is largely limited.

Physically-based BRDFs [10], [19] are based on the principles of physical optics and provide a highly realistic representation of material reflectance properties. In comparison with empirical BRDFs, they are more computationally complex. As a rule, physically-based BRDFs require calculation of the microfacet (specular surface micro-areas) distribution function D, the function of light shadowing and masking by microfacets G, and the Fresnel coefficient F, which determines the ratio of reflected light depending on the angle of light incidence and material properties. Physically-based BRDFs of this type are based on the Cook-Torrance BRDF (F_{CT}), which is calculated according to the formula [11], [20]

$$F_{CT} = (D \cdot F \cdot G)/(4 \cdot \cos(\theta_i) \cdot \cos(\theta_o)). \quad (5)$$

Physically-based BRDFs are common in the systems of highly realistic rendering. However, in the case when it's needed to create the image of the highest quality, the mentioned BRDFs do not always provide reproduction of the reflective properties of materials with the needed level of accuracy. In such cases, the use of analytical BRDFs is not enough and it's necessary to use measurement-based BRDFs. Measurement-based BRDFs lie in the usage of large tables with the experimentally obtained BRDF values. Since the real BRDF values are used, the formed images are characterized by a high realism level. Moreover, unique patterns of light reflection from different materials are reproduced.

For example, a well-known measurement-based BRDF is the Matusik BRDF [10] [11]. In order to obtain the table of BRDF values, the measurement system was used, which is based on the image analysis. The measurement system included a stationary camera, a rotating table for the material, a piece of material of spherical form, and a light source, which was rotating around the material. 330 images of high-dynamic-range (HDR) were obtained during the measurement for each material. After this, the BRDF value was calculated relative to each pixel of the HDR-image, taking to account the data of ray intersection with the material sphere in the respective point. After obtaining BRDF values, they were statistically processed, including the noise reduction.

The Rusinkiewicz coordinate system [21] is used for the parameters of measured BRDF values, it provides a more accurate representation of the specular highlight at the surface of the material. This coordinate system involves the use of the halfway vector $\vec{H}$ and vector $\vec{D}$ (obtained by rotating $\vec{L}$ into the coordinate system, where $\vec{H}$ coincides with $\vec{N}$). Each material table contains 1458000 cells relative to 90 levels of the θ_h angle values, 90 levels of the θ_d angle values, 180 levels of the ϕ_d angle values (θ_d, ϕ_d are spherical coordinates of the $\vec{D}$ vector). As a result, the tables of measured isotropic BRDF values for 100 materials were formed. This set of tables with measured BRDF values is known as the MERL database.

A big disadvantage of the Matusik BRDF and, overall, of measurement-based BRDFs, is a large size of the tables. The Matusik BRDF is characterized by a total size of 100 material tables in 3.25 Gb. Moreover, access to the tables of high dimensionality is usually characterized by high computational requirements. In particular, local scene data should be transformed into table indexes, and interpolation of BRDF values relative to missing parameter values is required. Therefore, the tasks of compact representation of measured BRDF values and providing an effective data access are relevant.

The classical directions of compact representation of measured BRDF values tables are the data-based formation of analytical BRDFs (object visualization quality decreases, it's hard to select parameters), the use of sums of individual functions, products of functions, wavelets, spherical harmonics, and matrix factorization methods.

A promising direction is the representation of the measured BRDF values tables using neural networks. In this case, it is only necessary to store a relatively small number of neural network weights, which in connection with input scene parameters provide a quite accurate prediction of BRDF values. In addition, neural networks are universal function approximators, provide a high calculation parallelization, and don't require constructing the form of table data representation by hand, which is learned by the network. Neural representation of BRDF values is considered as a distinct type of BRDFs.

One of the methods of neural representation of BRDF values (NBRDF) [8] was proposed by A. Sztrajman et al. A multilayer perceptron (MLP [22], [23]) with two hidden layers is used for predicting BRDF values relative to surface point data. A vector of dimensionality 6×1 with the coordinates of vectors $\vec{H}$, $\vec{D}$ at the surface point is used as the input to the neural network. Hidden layers have dimensionality 21×1, after them the activation function ReLU is used. The final layer has

dimensionality 3×1 and corresponds to the BRDF value for each RGB-channel. An exponential activation function is used for the final layer. Fig. 2 shows the MLP architecture used in the NBRDF method.

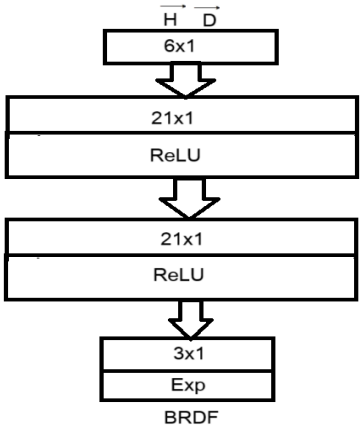


Fig. 2. **Architecture used in the NBRDF method**
***Source*: adapted by the authors from [8]**

Neural network training was conducted relative to 100 materials from the MERL database. As a result, 100 files with neural network parameters (weights and biases), corresponding to each material, were formed. Each file contains 675 parameters. Accordingly, 100 files overall contain 67500 parameters and take up 1.95 Mb. Additionally, the authors of the method have proposed to encode each block with 675 parameters by 32 parameters using the autoencoder. However, the number of decoder parameters was 71475. Additionally, neural network training respective to other datasets, such as Nielsen and RGL, was examined.

Therefore, the advantages of this method are the small size of the neural network, compact representation of BRDF values, high speed of BRDF values calculation, which is comparable with analytical models. The disadvantage is the use of 100 blocks of data (in the case of the MERL database representation) with neural network parameters. Blocks of parameters take up relatively small memory volumes, but if the modification of the neural network architecture is needed, each block should be formed from scratch.

Consequently, it is advisable to additionally use a vector of material features as input to the neural network, this makes it possible to store only one block of parameters. Learned latent vectors are usually used as vectors of material features.

Despite the highest accuracy of representing reflective properties of materials, latent vectors are characterized by a number of disadvantages:

1. Latent vectors of features, which are stored for further usage in some external file, are dependent on a particular neural network architecture and the process of its training. If the architecture of neural network is changed, they lose the validity and should be recalculated again.

2. Introducing additional blocks for generating material feature vectors or neural network weights can significantly increase computational complexity.

For example, the hypernetwork-based model Hyponet [9] (see below) contains additional 10 blocks with three layers for the determination of the respective weights of the main neural network.

3. Latent vectors don't have a physical meaning. At the same time, the desirable characteristic features of all BRDF types are expressivity and connection with real properties of materials.

Instead of that, physically meaningful material features are universal and can be used in different neural architectures without recalculations and without introducing additional computational blocks. Therefore, the use of physically meaningful material features is more appropriate and productive if the accuracy of BRDF values predicting is sufficient.

Additionally, a perspective compromise option between using a high number of files with neural network parameters and using a vector of material features is training neural networks respective to clusters of materials. In this case, a significantly lower number of parameter files is used, and the vector of material features is small or not used at all.

If the main task is a maximally accurate representation of the original table of BRDF values, time of scene visualization is not significantly limited, it's optimal to use hypernetworks. A hypernetwork is a neural network, which generates weights of other, main neural network.

For example, the hypernetwork, proposed by A. Sztrajman, F. Gokbudak et al. [9], is used for generation of neural BRDF parameters, corresponding to a particular material. One of the main advantages of the method is a highly accurate prediction of BRDF values for new materials, relative to which the training of model was not conducted. Overall, the three neural networks are used: an encoder for transforming N pairs of $\vec{H}$, $\vec{D}$ coordinates and respective BRDF values into a latent vector of dimensionality 40×1 (alternatively 6×1), a hypernetwork-decoder for transforming latent vector of material features into parameters W of the main neural network, and a main neural network for predicting BRDF values. The encoder is a MLP with two hidden layers of dimensionality

ISSN 2663-0176 (Print)
ISSN 2663-7731 (Online)

128× 1. The encoder is used for every pair of coordinates and BRDF values, after which the obtained latent vectors are averaged. The decoder contains 10 neural MLP-blocks with three layers for predicting neural network parameters. In general, main neural network Hyponet corresponds to the NBRDF architecture, but contains 3 hidden layers of dimensionality 60×1, the activation function ReLU is used after the final layer. Fig. 3 shows the neural architecture used in this method.

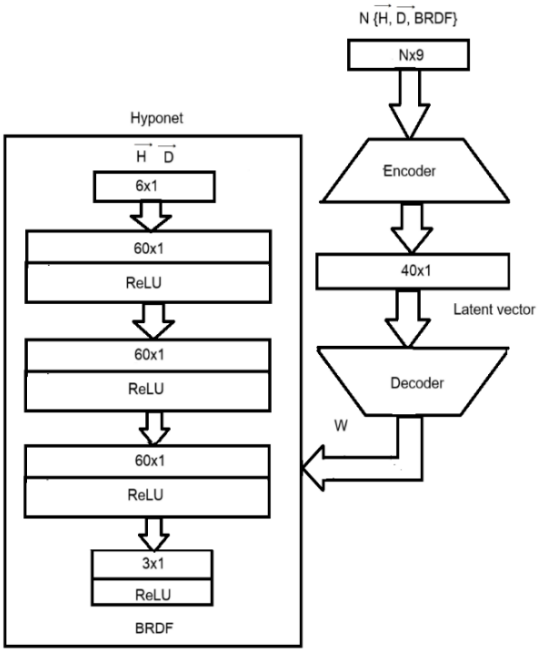


Fig. 3. **Architecture for hypernetwork-based prediction of BRDF values**
***Source*: adapted by the authors from [9]**

Since the measured BRDF values in the MERL database are characterized by a high-dynamic-range, in order to increase the accuracy of neural network training, these values were transformed using the special expression [9]

$$\ln\left(\frac{RFL+0.002}{RFL_{ref}+0.002}+1\right), \quad (6)$$

where RFL is value of BRDF, RFL_{ref} is reference value of BRDF (for example, median or average BRDF value respective to the angle θ_i).

However, BRDF values transformation expressions are characterized by different effectiveness respective to different material types (for example, for diffuse and specular [24] materials). Consequently, the adaptive combining of transformation expressions for BRDF values depending on material properties is reasonable.

Let us summarize the main discussed methods of representing BRDFs in the Table 1.

Table 1. **Methods of BRDF representation**

Method/ BRDF repre-sentation type	Material param-eters/ repre-sentation size	Memory require-ments/ prediction computa-tional complexity	Accu-racy	Multiple material repre-sentation
Lambert/ analytical	1	Very low/ very low	Mod-erate	Yes
Blinn-Phong/ analytical	1	Very low/ low	Mod-erate	Yes
Cook-Torrance/ analytical (physical-ly based)	Few	Low/ low-moderate	High	Yes
Measured tabular BRDF/ measured	Large number of samples	High/ high	Very high	Separate per material
NBRDF/ neural	Material-specific weights	Moderate/ low-moderate	High	Separate per material
Hyponet/ neural	Generat-ed weights	Moderate-high/ moderate-high	High	Yes

***Source*: compiled by the authors**

The analysis shows that existing neural-network-based BRDFs provide a compact and highly accurate representation of the reflective properties of materials but still have limitations. Therefore, the improvement of existing neural BRDFs is relevant: use of the single set of parameters and use of the vectors with physically meaningful material features for more resource effective BRDF value prediction, and adaptive combining of transformation expressions for a more accurate BRDF values prediction.

THE AIM OF THE STUDY

The aim of the study is to increase the efficiency of neural BRDF prediction by developing models that use a single set of neural network parameters for a fixed set of materials, reducing the number of neural parameter sets through material clustering, and adaptively combining BRDF value transformation functions to improve the prediction of high-dynamic-range BRDF values.

DATASET STRUCTURE

In this study, the processed database of measured BRDF values MERL is used. During preprocessing, the MERL BRDF tables were

converted into individual samples containing the coordinates of $\vec{H}$, $\vec{D}$ vectors, corresponding BRDF values for each RGB-channel, and the cosine of the angle between $\vec{L}$, $\vec{N}$ vectors. The unused components of the original data representation were excluded.

The dataset is divided into 100 MERL materials. The data of 90 materials are used for neural model training (85 % of samples) and validation (15 % of samples), the data from 10 materials are used as the test dataset. Moreover, for each training material, 15 % of samples were moved to the second test dataset. Accordingly, the second test dataset is used to evaluate how accurately the model predicts values for vector pairs, which were not used during training.

NEURAL BIDIRECTIONAL REFLECTANCE DISTRIBUTION FUNCTIONS BASED ON PHYSICALLY MEANINGFUL MATERIAL FEATURES

We augment the input data of the neural network for the prediction of BRDF values with the material features vector. It gives the possibility to use only one file with neural network weight parameters instead of a large number of files, corresponding to each material. A vector with physically meaningful material features is used as the features vector. In comparison with latent vectors, the advantages of using vectors of this type are the presence of physical meaning of the data, no necessity to introduce additional computational blocks, universality of features and their independence from the neural network architecture.

For the further comparison of results, we firstly examine the results of applying the original NBRDF neural network [8] to learning the reflective properties of each material from the MERL dataset. In the Table 2, material names and the respective validation errors of BRDF values prediction (relatively to the new vector pairs, the best values from 3 attempts) are provided. Only the materials with the 10 best and 10 worst error values are listed.

The following expression [8] is used as the training and validation error

$$\left|\begin{matrix}\ln(1 + RFL_{true} \cdot \cos(\theta_i)) - \\ -\ln(1 + RFL_{pred} \cdot \cos(\theta_i))\end{matrix}\right|, \qquad (7)$$

where RFL_{true} is target BRDF value from the table of measured data, RFL_{pred} is predicted by neural network BRDF value.

As shown in the table, the accuracy of NBRDF depends on the represented materials. Overall, the average validation error of BRDF values prediction by NBRDF for 100 MERL materials is 0.0012. The highest error value – 0.0077. Therefore, a neural model which uses a single set of weights for all materials should provide a BRDF value prediction error that is comparable with 0.0012 and is not higher than 0.0077.

Table 2. **Validation errors of BRDF values prediction by the original neural network NBRDF for different materials**

Material name	Validation error	Material name	Validation error
Black-fabric	0.0002	Pink-felt	0.0017
Black-obsidian	0.0003	Silver-metallic-paint	0.0017
Light-brown-fabric	0.0003	Silver-metallic-paint2	0.0023
Black-soft-plastic	0.0004	Delrin	0.0024
Blue-fabric	0.0004	Grease-covered-steel	0.0024
Dark-blue-paint	0.0004	Nylon	0.0028
Color-changing-paint3	0.0004	Polyethylene	0.0030
Dark-specular-fabric	0.0004	Steel	0.0062
Green-metallic-paint2	0.0004	Red-phenolic	0.0065
Red-fabric	0.0004	Yellow-phenolic	0.0077

***Source*: compiled by the authors**

Additionally, the architecture of NBRDF, which is used in the study, was slightly modified through the analysis of mean validation errors of BRDF values prediction respective to 5 randomly chosen materials. It was found that increasing the number of hidden layers to 4 led to some decrease in the mean validation error to 0.0008. Additionally, different activation functions for the final layer of neural network were studied. As a result, it was decided to use, as in the original study, the exponential activation function. The use of the SoftPlus function provided a similar validation error. Noticeably worse values were obtained while using ReLU and SoftSign functions.

Before the study of the use of vectors with physically meaningful features, we analyze the results of neural network training relative to all materials without using material feature vectors. In effect, the whole set of training materials is considered as one cluster of materials. The training error of BRDF values prediction is 0.0229,

ISSN 2663-0176 (Print)
ISSN 2663-7731 (Online)

validation error is 0.0229, and the test error relative to 10 materials is 0.0192.

We consider the use of an input vector of material features, which contains the values of the surface shininess coefficient, the refraction coefficient, and the intensity of the base material (relative to the 3 RGB channels). Surface shininess coefficient is used in the empirical BRDFs for controlling the specular highlight concentration level at the surface of an object (alternatively, the surface roughness coefficient, which is used in the microfacet BRDFs, can be applied). The light refraction coefficient is used for the Fresnel coefficient calculation in the microfacet BRDFs. The base color determines the color of the material surface.

These features were chosen because they enable material identification within existing analytical BRDFs by determining specularity, light interaction peculiarities, and diffuse albedo of the surface. In addition, they provide an opportunity to compactly represent the reflective properties of materials using directly interpretable quantities.

The values of these features were obtained from the special tables (particularly, [25], [26]), and were approximately estimated using the GPT-5 model. The prompt included a request to estimate the corresponding features using the provided reference values from [25], [26]. Values were checked by three lecturers of the Department of Software of Vinnytsia National Technical University, who teach computer graphics and scientific visualization, and adjusted if necessary. Accordingly, GPT-5 was used as an auxiliary tool for initialization.

In Table 3, the examples of used values of the surface shininess coefficient, refraction coefficient, and base color intensity are provided.

Table 3. **The examples of used feature values**

Material	Surface shininess coefficient	Refraction coefficient and base material color values		
		R	G	B
Black-obsidian	300	1.500/ 13	1.500/ 13	1.500/ 20
Chrome	600	2.025/ 217	2.789/ 217	2.025/ 230

***Source*: compiled by the authors**

Examples demonstrate that the selected features enable the differentiation of materials with varying optical and color properties.

Since in this case the dimensionality of the neural network input layer increases to 13× 1, we scale the dimensionality of the four hidden layers to 45× 1. Then, the total number of neural network parameters is 6978. The parameters are stored in a single file of size 110 Kb, which is 18 times less in comparison with the NBRDF method.

Min-max normalization was applied to all input data of the neural network. Neural network training was conducted in the Kaggle environment using a CPU (batch_size=1024). In all experiments in the article, Keras 3.5 library and Adam optimizer were used, and model training was performed at least three times. Fig. 4 shows the plot of training and validation error change during the neural network training.

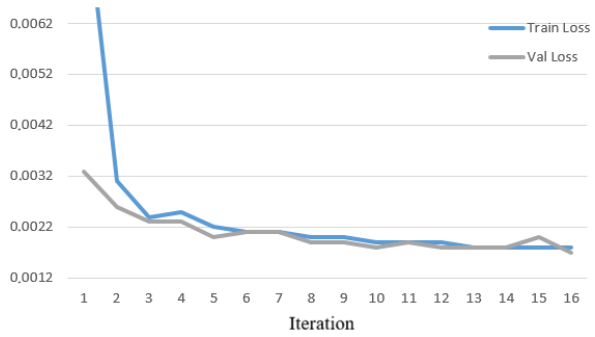


Fig. 4. **The plots of training and validation error of BRDF values prediction during the use of material reflectance features**

***Source*: compiled by the authors**

After 16 iterations, the training and validation errors of BRDF values were respectively 0.0018 and 0.0017. The errors are slightly larger than the average error of neural network training relative to every material (0.0012), but are lower than the determined maximal acceptable error of 0.0077.

The test error relative to the new coordinates of the vectors $\vec{H}$, $\vec{D}$, which were not used during the neural network training, was 0.0017. The test error relative to the new materials was 0.0314. Therefore, in this case the use of the physically meaningful features instead of latent vectors provides a quite accurate prediction of BRDF values respective to the used during the training materials. Moreover, the neural model has a good generalization relative to the new coordinates of $\vec{H}$, $\vec{D}$. However, if the MERL database is supplemented with new materials, this method cannot be applied. In such a case, latent vectors should be used for the representation of material properties.

It's important to note that a large subset of famous measured BRDF value datasets is not supplemented with the new materials. Therefore, the accurate BRDF values prediction relative to the new pairs of $\vec{H}$, $\vec{D}$ is enough. Additionally, such datasets are often combined with each other. Then, it's reasonable to train the neural network with the use

of physically meaningful material features relative to each material dataset.

Next, we use the 16 descriptive features [27], which were proposed by W. Matusik for the MERL-based synthesis of new materials, as the input vector of material features. The set of 16 descriptive features includes [27]: redness, greenness, blueness, specularness, diffuseness, glossiness, metallic-like, plastic-like, roughness, silverness, gold-like, fabric-like, acrylic-like, greasiness, dustiness, rubber-like. These 16 features were selected because they provide a comprehensive representation of the visual properties of the materials in the MERL database.

In order to obtain the values of the 16 descriptive material features on a scale of $[0, 5]$, the GPT-5 model was used. The values were generated relative to material names and similarly checked and adjusted by three lecturers. In the Table 4, the examples of the 16 used descriptive feature values for the three materials are provided.

Table 4. **The examples of the 16 used descriptive feature values for the three materials**

Material	Red-ness/ green-ness/ blue-ness/ specular-ness	Diffuse-ness/ glossi-ness/ metallic-like/ plastic-like	Rough-ness/ silver-ness/ gold-like/ fabric-like	Acrylic-like/ greasi-ness/ dusti-ness/ rubber-like
Red-fabric	5	5	4	0
	0	0	0	0
	0	0	0	3
	1	0	5	0
Pink-plastic	4	3	2	2
	0	3	0	1
	0	0	0	2
	3	5	0	0
Nickel	0	1	1	0
	0	5	4	1
	1	5	0	2
	5	0	0	0

***Source*: compiled by the authors**

The examples demonstrate that the selected 16 material features provide a more detailed representation of the material reflective properties than the 7 physically meaningful features.

In this case, the dimensionality of the neural network input layer is 22×1, so the dimensionality of the four hidden layers is scaled to 77×1. The neural network has 20023 parameters, which are stored in a file of size 260 Kb (8 times less in comparison with the NBRDF method).

Similarly, min-max normalization was applied to the neural network input data, the training was conducted with the use of CPU in the Kaggle environment (batch_size=1024). Fig. 5 shows the plots of the training and validation errors during the neural network training.

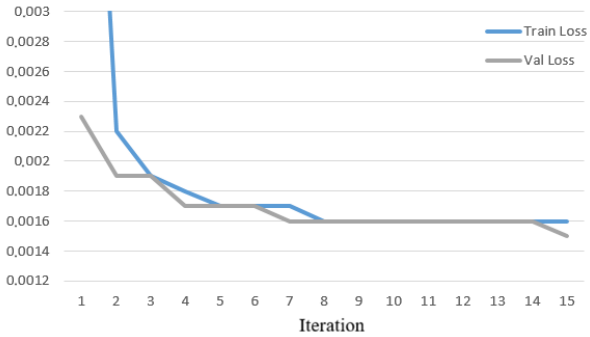


Fig. 5. **The plot of change of the training and validation errors of the BRDF values prediction during the use of the descriptive material features**
***Source*: compiled by the authors**

After the 15-th training iteration, the training error was 0.0016, and the validation error was 0.0015. The error of the BRDF values prediction relative to the new pairs of $\vec{H}$, $\vec{D}$ was 0.0014, and relative to new test materials – 0.0281.

To assess the impact of the proposed physically meaningful features on the accuracy of predicting BRDF values, the results of training neural models relative to 7 and 16 proposed characteristics were compared. When using 7 physically meaningful features, the test errors for new pairs of vectors and new materials were 0.0017 and 0.0314, respectively. When using 16 features of W. Matusik, the test errors were 18 % and 11 % lower – 0.0014, 0.0281, respectively. At the same time, this increase in the accuracy of predicting BRDF values was achieved by increasing the number of neural network parameters almost threefold – from 6978 to 20023.

The time of BRDF values prediction by the proposed models was examined in the Kaggle environment (CPU) respective to 10 million material test samples.

The time of BRDF values prediction by the 7-feature-based model was 8 s, and by the 16-feature-based model – 13 s. In comparison, the time of values prediction by the hypernetwork-based model with the additional computational blocks was 18-62 s (depending on the number of samples, see the following sections).

Additionally, the use of a significantly larger MLP (6 layers with 128 neurons and a skip connection) – as employed in [21] – was tested for predicting BRDF values using 7 and 16 physically

ISSN 2663-0176 (Print)
ISSN 2663-7731 (Online)

meaningful material features. The test error for new vector pairs was substantially lowers (0.0008–0.00012), while the error for new materials ranged from 0.0186 to 0.0228. However, the number of parameters was considerably higher (71028-72195), and the prediction time for 10 million samples (CPU) was approximately 33-35 s. Consequently, given enhanced hardware capabilities, employing larger MLPs may be advisable.

The test figure "Dinosaur" was visualized using the proposed neural models in the 3D-rendering software tool Idx3d. Fig. 6 shows the results of the test figure visualization using the neural network with the use of 7 material features and the neural network with the use of 16 material features.

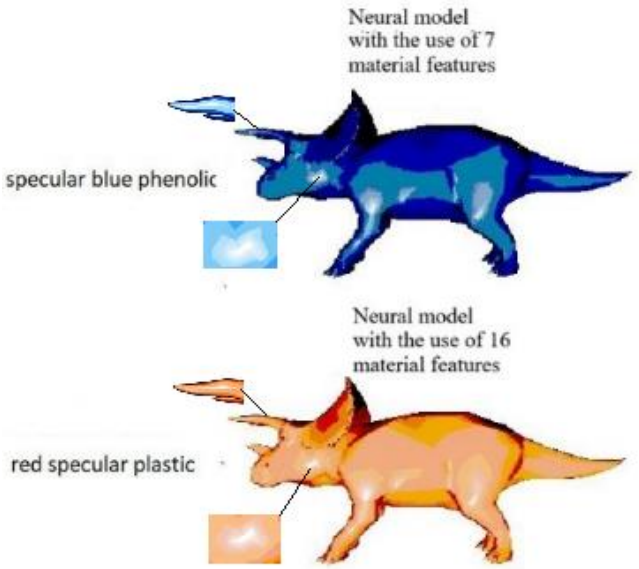


Fig. 6. **Results of the test figure visualization, using the proposed neural models**
***Source*: compiled by the authors**

The analysis has shown that the average NMSE (Normalized Mean Squared Error) metric value between the MERL-tables-based images and the proposed-models-based images is approximately 0.001. It means that the significant differences between images are not present.

Therefore, the use of neural networks with the physically meaningful material features provides a highly productive, quite accurate and compact representation of the fixed sets of measured BRDF values.

The absence of the necessity to introduce new computational blocks for the determination of latent vectors gives the possibility to increase the productivity of BRDF value prediction. The use of a single neural network parameter set provides more resource efficient neural network usage.

NEURAL BIDIRECTIONAL REFLECTANCE DISTRIBUTION FUNCTIONS BASED ON THE MATERIAL CLUSTERS

Grouping materials into clusters gives the possibility to operate with a significantly smaller number of parameter files than when training the neural network relative to each material. Moreover, a relatively small number of material features is used.

We analyze six methods of forming material feature vectors for subsequent clustering.

The first method involves the use of the pyramidal encoder of the measured BRDF values table, proposed by the authors. The N samples of the $\vec{H}$, $\vec{D}$ coordinates and the respective BRDF values are used as the encoder input. The set of samples is transformed into a 1D-vector, from which the groups of 405 numbers are extracted. If necessary, the groups are padded with zeros.

Next, the MLP with two hidden layers of dimensionality 128×1 and a final layer of the final latent vector dimensionality is applied to each group. Different MLP weight parameters are used at each level of detailization.

The obtained intermediate latent vectors are merged into a 1D-vector, after that the groups of 405 numbers are extracted again. This process is repeated, until the size of the formed 1D-vector is lower than 405 elements.

Then, the 1D-vector is padded with zero values, after that the processed data are transferred to the final latent vector. Fig. 7 shows the example of the gradual change in the dimensionality of data by the encoder when $N = 90$.

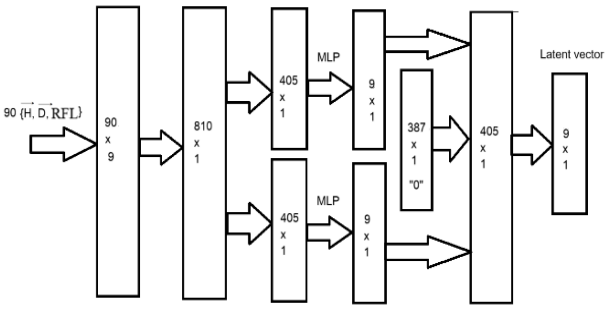


Fig. 7. **The example of data dimensionality change by the encoder**
***Source*: compiled by the authors**

The second method involves the use of 16 descriptive material features, the third method – the use of NBRDF weight parameters [8], obtained for each material. The fourth method involves the use of the encoder for the hypernetwork, proposed by F. Gokbudak, A. Sztrajman et al. [9] (see the Literature

Analysis). An MLP is applied to each dataset sample, after that the obtained intermediate latent vectors are averaged. The fifth method involves merging the latent vectors, obtained by the fourth and first methods. The sixth method involves the use of the encoder, proposed by C. Zheng et al. [28] for the compact representation of the material reflectance properties. Similarly, the MLP with the dimensionalities of layers 400×1, 400×1, 400×1, 64×1 is applied to each dataset sample, then the encoded samples are averaged. The averaged vector is used as the input of the MLP-aggregator with the layers of dimensionality 128×1, 128×1. The statistical mean and the covariance are predicted at the output of the MLP-aggregator for the further generation of the latent vector of dimensionality 6×1. The specified parameters are used in the study.

Using the material features, obtained using the specified six methods, the MERL materials were clusterized into 9 and 15 uniform clusters. The k-means algorithm was used for the clustering.

The training of the neural network, the architecture of which corresponds to NBRDF, was conducted in the Kaggle environment (CPU, batch_size=1024) relative to each formed material cluster. As a result, it was found that the mean validation error was 0.0089 – 0.0211 during the neural network training relative to each of the formed clusters, depending on the method of their formation. These values are higher than the maximal validation error of neural network training relative to each material (0.0077).

Thus, we clusterize the materials, taking into account the results of the neural network training relative to different numbers of original clusters and methods of their formation.

For this, we execute the following sequence of steps:

1. We sort all candidate clusters by the validation error of BRDF values prediction.

2. Duplicate materials are removed from the clusters.

3. The validation error of neural network training relative to each updated candidate cluster is determined. The mean weighted validation error relative to the set of clusters is calculated.

4. For each cluster the most similar one is selected through the comparison of the mean latent vectors of clusters, formed using the first, fourth and sixth methods. The comparison is done by computing the Euclidean distance.

5. The pair of clusters, the unification of which provides the lowest validation error of the neural network training, is selected. As a result, a new cluster is formed.

6. The steps 4-5 are repeated, until the mean weighted validation error relative to the set of clusters becomes higher than 0.0077 (a slight excess of this value is acceptable for particular clusters).

After the execution of step 3, the set of materials was divided into 30 clusters. The mean weighted validation error of the neural network training relative to the formed clusters was 0.0060. After the execution of the steps 4-6, number of clusters was decreased to 18 with the mean weighted validation error of 0.0077.

The clustering of materials is performed as a separate preprocessing step before the use of cluster-based neural BRDFs. Thus, cluster formation is not repeated during each neural BRDF run. To evaluate the consistency of the cluster formation procedure, the neural models were trained three times for the candidate clusters. Validation error is a central criterion for sorting and merging clusters in the proposed algorithm. Therefore, the consistency of validation errors (with an average absolute deviation of $9\cdot 10^{-5}$) indicates that the aforementioned decisions of the algorithm are not significantly affected by variations in model training.

The formed material clusters and the respective validation errors of BRDF values prediction are provided in the Table 5. The final composition of 18 material clusters was obtained using the proposed clustering procedure. Validation errors show the prediction accuracy of the neural models trained for each cluster. As a result of the analysis of the formed clusters, it is determined that the main factors of clustering were the material type, material color, and surface specularity level. In particular, the reason for the significant contribution of the material color to the clustering result is that the full expression of BRDF calculation includes not only the specular BRDF-component, but also the values of the diffuse and specular albedos.

It is evident that since the base color of the material is taken into account, the color correction of the predicted BRDF value relative to the material of the cluster is needed. Accordingly, the validation errors of the neural network training with consideration of the base color vectors for the cluster materials are also provided in the Table 5. Then, the mean weighted validation error of BRDF values prediction decreases to 0.0024.

ISSN 2663-0176 (Print)
ISSN 2663-7731 (Online)

Table 5. **Formed clusters of the MERL materials**

No.	Set of cluster materials	Validation error of BRDF values prediction relative to the cluster of materials (without/with considering the vector of base color)	No.	Set of cluster materials	Validation error of BRDF values prediction relative to the cluster of materials (without/with considering the vector of base color)
1	ss440, steel, chrome-steel, tungsten-carbide, chrome, green-metallic-paint2, black-fabric, black-phenolic, specular-black-phenolic, specular-blue-phenolic, specular-green-phenolic, hematite, black-obsidian, silicon-nitrade	0.0033/0.0011	10	pink-fabric, pink-felt, white-fabric, nylon, pure-rubber	0.0081/0.0028
2	brass, grease-covered-steel, red-metallic-paint, blue-metallic-paint2, specular-violet-phenolic	0.0058/0.0014	11	delrin, polyethylene, teflon	0.0092/0.0081
3	black-oxidized-steel, black-soft-plastic, dark-specular-fabric, light-brown-fabric, dark-blue-paint, cherry-235, special-walnut-224, color-changing-paint1, color-changing-paint3	0.0047/0.0009	12	light-red-paint, pink-fabric2, violet-rubber	0.0094/0.0015
4	yellow-paint, yellow-plastic, yellow-phenolic, specular-white-phenolic	0.0104/0.0025	13	silver-metallic-paint, two-layer-silver	0.0099/0.0041
5	gold-metallic-paint, gold-metallic-paint2, gold-metallic-paint3, natural-209, two-layer-gold, alum-bronze	0.0095/0.0018	14	pink-plastic, specular-yellow-phenolic, yellow-matte-plastic, orange-paint	0.0106/0.0016
6	red-specular-plastic, red-plastic, maroon-plastic, specular-red-phenolic, red-phenolic, specular-maroon-phenolic, specular-orange-phenolic, red-fabric, red-fabric2, dark-red-paint, purple-paint	0.0088/0.0021	15	gold-paint, pink-jasper	0.0096/0.0016
7	white-paint, white-acrylic, white-diffuse-bball, alumina-oxide	0.0065/0.0064	16	blue-rubber, green-latex, gray-plastic, white-fabric2, pickled-oak-260	0.0087/0.0016
8	green-plastic, green-acrylic, blue-acrylic, violet-acrylic, pvc, polyurethane-foam, green-metallic-paint, blue-metallic-paint, color-changing-paint2, fruitwood-241, colonial-maple-223, ipswich-pine-221, green-fabric, blue-fabric, aluminium, nickel, aventurnine	0.0099/0.0026	17	beige-fabric	0.0020
9	pearl-paint, silver-paint, white-marble, neoprene-rubber	0.0094/0.0057	18	silver-metallic-paint2	0.0023

***Source*: compiled by the authors**

Therefore, the base-color correction substantially reduces the validation error.

The dimensionality of the input layer of the proposed neural network is 9× 1 (including the base color), and the dimensionality of each of the two hidden layers - 32× 1. In this case, the use of the cluster-based neural BRDFs involves storing 18 files with 1475 parameters (total 26550 parameters of size 641 Kb). At the same time, the NBRDF method involves the use of 100 files with 675 parameters (total 67500 parameters of size 1.95 Mb). Among all proposed models, the cluster-based models are the most productive (the time of BRDF values prediction (CPU) relative to the 10 million samples was 3 s), as they involve the processing of a smaller number of the input material features.

In the software tool Idx3d, the image of the test figure "Dinosaur" was formed, using the proposed neural model, which is based on the material cluster. The visualization of the figure was done relative to the silver-metallic-paint material. The results of the visualization are shown in Fig. 8.

In comparison with the other proposed models, the cluster-based neural BRDFs are characterized by a less accurate representation of the material reflective properties. However, the quality of 3D figure visualization is still acceptable.

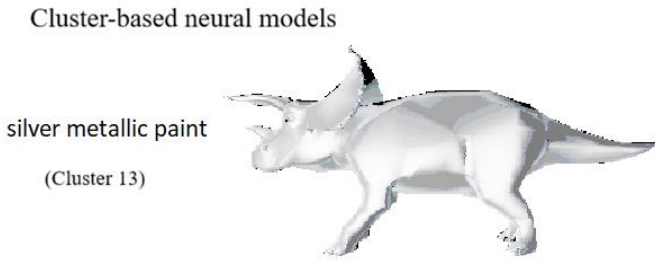


Fig. 8. **Results of the test figure "Dinosaur" visualization using the cluster-based neural model**
***Source*: compiled by the authors**

Therefore, the advantages of the cluster-based neural BRDFs are that they require a small number of input material features and the storage of a relatively low number of files with parameters. It gives the possibility to increase the productivity of BRDF values prediction and decrease the memory volume required for use.

The performance, accuracy, and total size of parameters for the proposed neural methods of compact BRDF representation are summarized in the Table 6.

Table 6. **Analysis of the proposed methods**

Method	Total size of parameters, Kb	Train/ val. error	Test error (new vectors/ materials)	Time of value prediction for 10 mln samples,s
Based on 7 physically meaningful features	110	0.0018/ 0.0017	0.0017/ 0.0314	8
Based on 16 descriptive features	260	0.0016/ 0.0015	0.0014/ 0.0281	13
Based on material clusters	641	0.0024 (avg. val. error)	N/A	3

***Source*: compiled by the authors**

The comparison shows that neural BRDFs based on physically meaningful material features enable the representation of various materials using a single model with a small number of parameters, whereas clustering-based neural BRDFs offer higher performance in predicting reflectance values. Thus, clustering-based BRDF models are advantageous when high prediction speed and compact model parameter representation are the priorities.

ADAPTIVE COMBINING OF THE TRANSFORMATION FUNCTIONS FOR INCREASING THE ACCURACY OF THE NEURAL BRDF VALUES PREDICTION

If it is important not only to provide a highly accurate prediction of BRDF values, but also to provide the ability of the model to quite accurately determine the values of BRDF relative to a material, which was not used during its training, then it's reasonable to use hypernetworks. A hypernetwork, using the sample of material data, predicts the weights of the main neural network, which predicts the BRDF value.

A correct processing of target values is important for the effective training of the hypernetwork and the main neural network. As a rule, the measured BRDF values are the high-dynamic-range values. In particular, the distribution of BRDF values from the training dataset by percentage intervals is provided in Table 7.

The majority of BRDF values are less than 1, whereas the remaining values are significantly larger. The non-uniformity of this distribution indicates the need to employ non-linear transformation expressions for more effective processing of BRDF values.

ISSN 2663-0176 (Print)
ISSN 2663-7731 (Online)

Table 7. **The distribution of BRDF values from the training dataset by ranges**

Range of BRDF values	Percent
0-1	99.66535 %
1-10	0.14454 %
10-100	0.13811 %
100-1000	0.04822 %
1000-10000	0.00378 %

***Source*: compiled by the authors**

In order to achieve a more accurate prediction of the BRDF values, transformation functions are applied to the target BRDF values during neural network training. We analyze the functions that can be used for the BRDF values transformation.

The first function $T1$ is based on the logarithmic transformation of the BRDF values, including the determined reference BRDF value. The function is calculated using the expression (6).

This function is used in the Hyponet method, proposed by F. Gokbudak, A. Sztrajman et al. [9].

The second function $T2$ involves the calculation of the square root of the BRDF value

$$T2(RFL) = \sqrt{RFL}. \quad (8)$$

The logarithmic expression of the third transformation function $T3$ [24], unlike the first transformation function, doesn't include the reference BRDF value

$$T3(RFL) = \ln(RFL + 1). \quad (9)$$

The fourth transformation function $T4$ [24] is also a logarithmic function and involves the scaling of the BRDF value using the $\cos(\theta_i)$ multiplier

$$T4(RFL) = \ln(RFL(\cos(\theta_i) + 0.001) + 1). \quad (10)$$

Moreover, the use of non-transformed BRDF values relative to the particular materials can be reasonable. Then,

$$T5(RFL) = RFL. \quad (11)$$

This set of transformation functions was chosen to provide a variety of compression and representation of BRDF values. The square-root function provides a less aggressive non-linear transformation of BRDF values. Logarithmic functions, with and without the use of reference values and with scaling coefficients, provide stronger compression of large values while providing various forms of normalization. In particular, the use of cosine multipliers is more appropriate for near-diffuse surfaces [24]. The use of reference values provides additional normalization of the BRDF values. Direct use of the BRDF values is appropriate for cases where the use of transformation expressions does not provide a gain in the prediction accuracy. Accordingly, the set provides complementary transformation behaviors, depending on the material reflective properties.

Different material types are characterized by different peculiarities of the light reflection. Accordingly, the efficiency of applying the particular transformation function depends on the material properties. Therefore, we represent the transformation expression of the BRDF values $T(RFL)$ as the weighted sum of the expressions $T1(RFL) - T5(RFL)$

$$T(RFL) = k1 \cdot T1(RFL) + k2 \cdot T2(RFL) + \\ + k3 \cdot T3(RFL) + k4 \cdot T4(RFL) + k5 \cdot \\ T5(RFL), \quad (12)$$

where $k1$- $k5$ are weight coefficients, which are learned.

Taking into account the given expression, we modify the neural method Hyponet for the BRDF values prediction. A new MLP-type neural network that predicts the coefficients $k1$- $k5$ using the samples of the measured BRDF values is introduced.

The architecture of the additional neural network is based on the architecture of the original neural network encoder [9]. The additional neural network includes the input layer, two hidden layers of dimensionality 128×1, after which the activation function ReLU is used, and the final layer of dimensionality 5×1, after which the activation function SoftMax is used. Accordingly, the percentage coefficients are determined for every transformation function. The neural network is applied to each material sample, and the resulting sets of coefficients are then averaged. Fig. 9 schematically shows the process of transformation of one sample of the material data into the set of percentage coefficients of the transformation function.

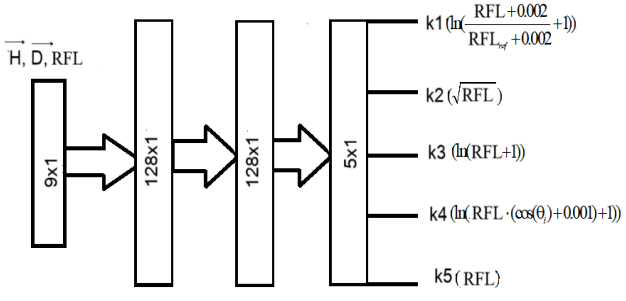


Fig. 9. **The schematic example of the material data sample transformation into the set of percentage coefficients of the transformation function**

***Source*: compiled by the authors**

We compare the results of the training of the original neural model based on the hypernetwork

and the neural model with the additional block of the transformation function coefficients determination. The training of both models was conducted during 400 iterations in the Kaggle environment with the use of P100 GPU. 15 materials from the 90 training materials were used for the model validation.

The expression from the original study [9] is used as the error function for minimization

$$\left|RFL_{true} \cdot \cos(\theta_i) - RFL_{pred} \cdot \cos(\theta_i)\right|, \quad (13)$$

where RFL_{true}, RFL_{pred} is the RGB-channel value of the target and predicted BRDF respectively (both values are in the transformed scale). The error is averaged over the number of training samples and materials, the regularization terms that are based on the weights, predicted by hypernetwork, and on the latent vector, formed by the hypernetwork encoder, are added to it.

The expression (7) is used as the error metric. The error metric shows the deviation between the predicted and target values of BRDF in the original scale.

Fig. 10 shows the plots of the validation error change for the original and modified neural models.

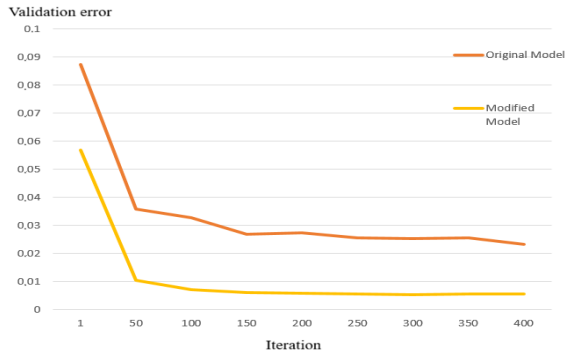


Fig. 10. **The plots of the validation error change for the original and modified neural models**
***Source*: compiled by the authors**

Fig. 11 shows the plot of the test metric change for the original and modified neural models relative to the new materials. The set of 10 test materials included aluminium, black-obsidian, blue-fabric, blue-metallic-paint, chrome, green-latex, natural-209, silver-metallic-paint2, white fabric2, yellow-matte-plastic. Therefore, the test dataset includes the materials of different types: metals, fabrics, paints, plastics.

In Table 8, the validation error and test metric values for the original and the modified neural models after 400 training iterations are provided. The table shows that the adaptive combination of transformation functions reduces the test metric for new materials from 0.0072 to 0.0063, compared to the original Hyponet model.

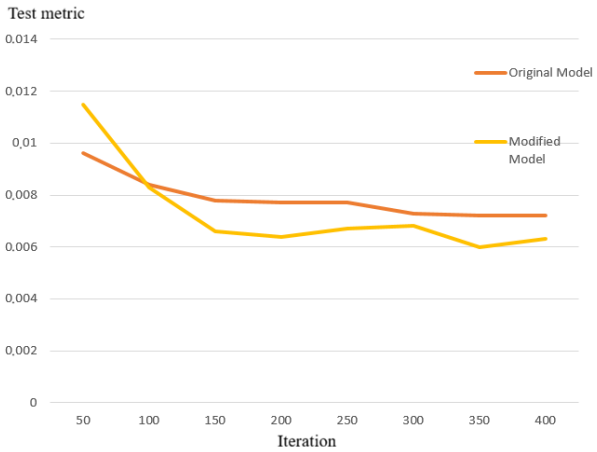


Fig. 11. **The plots of the test metric change for the original and modified neural models relative to the new materials**
***Source*: compiled by the authors**

Table 8. **The values of the validation error and the test metric for the original and modified neural models**

Function	Original model	Modified model with the adaptive combining of the transformation functions
Validation error at the training stage	0.0234	0.0056
Test metric relative to the new materials	0.0072	0.0063

***Source*: compiled by the authors**

Therefore, as a result of applying the adaptive combining of the transformation functions, the validation error was decreased by 4 times during the training, and the test metric of BRDF values prediction relative to the new materials was decreased by 12.5 %.

Additionally, the time of BRDF values prediction by the original and modified models relative to the 10 million test samples in the Kaggle environment (CPU) was examined. In the case of the full material dataset usage, the time of the BRDF values prediction by the original model was 57 s, by the modified model – 62.1 s, when using 10000 material samples for each material – 18.9 and 22.3 s respectively, when using only 40 samples – 18 and 20 s respectively.

It's worth mentioning that for a fixed neural network architecture, inference complexity is linear, specifically $O(N \cdot P)$, where N and P represent the number of samples and the number of neural network operations to process one sample,

ISSN 2663-0176 (Print)
ISSN 2663-7731 (Online)

respectively. Experiments conducted in the Kaggle environment using CPUs demonstrated that the proposed models perform quite efficiently without specialized hardware. However, for optimal processing of input samples in real-time systems, the use of modern Nvidia GPUs with CUDA support is recommended. The following considerations apply to all modified neural BRDFs mentioned in the study.

During the use of the modified neural model, firstly the weights of the transformation function coefficients are determined, using the subset of material data samples (vectors $\vec{H}$, $\vec{D}$ and BRDF values). Then, the vector coordinates and BRDF values, transformed by the combined function, are used as the input of the encoder. The latent vector, formed by the encoder, is used by the decoder for predicting the main neural network weights. The main neural network predicts the BRDF values that are transformed to the original scale, using the inverse combined transformation function.

Fig. 12 shows the example of the 3D-figure "Dinosaur" visualization in Idx3d using the modified neural model. The yellow-matte-plastic material was used for the visualization. The proposed model ensures a sufficiently accurate reproduction of reflectance patterns, which is consistent with the values presented in Table 6.

The analysis has shown that the average value of the NMSE metric relative to the 10 test materials was decreased by 12 %.

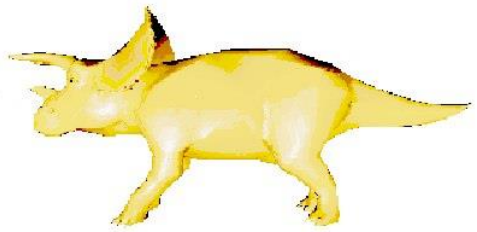


Fig. 12. **The test figure "Dinosaur", visualized in Idx3d using the modified neural model**

***Source*: compiled by the authors**

Therefore, the adaptive combining of the transformation functions at the neural network training stage provides a more correct BRDF values prediction relative to the new materials.

CONCLUSIONS

In the article, modified neural models for increasing the accuracy, performance and resource efficiency of BRDF values prediction are proposed.

The use of neural BRDFs based on physically meaningful material features is proposed. In comparison with the original NBRDF method, a single parametric file instead of 100 files with the neural network parameters is used, which gives the possibility to decrease the size of stored data by 8-18 times. The use of vectors with the physically meaningful material features provides a more productive and resource efficient BRDF values prediction relative to the fixed material datasets. In comparison with the Hyponet model that involves the latent-vector-based determination of optimal weight parameters in the additional block, the BRDF values prediction is more productive by 1.4-2.3 times. Since the physically meaningful material features have a physical meaning, they do not need to be recalculated in the case of neural network architecture change. Through the analysis of the NMSE metric, it is found that the quality of 3D-figures visualization using the proposed models is acceptable.

Additionally, the material-cluster-based neural models, the advantages of which are the use of a small number of files with neural network parameters and a small vector of material features, are proposed. In comparison with the NBRDF method, 18 files with the weight parameters are used, which provides a threefold reduction in stored data size. In comparison with Hyponet, BRDF values prediction is 6 times faster.

The increase in the accuracy of the BRDF values prediction relative to the new materials by 12.5 % is provided through the adaptive combining of the transformation expressions at the stage of training. Additionally, the use of the modified Hyponet model provided the decrease in the NMSE metric of visualization error by 12 % compared to the original model.

The proposed models have several limitations. Neural BRDFs based on physically meaningful material features are primarily applicable to a fixed set of materials. The accuracy of cluster-based neural BRDFs depends on the set of materials in each cluster and may be lower compared to other neural models. Adaptive combining of the BRDF value transformation functions introduces an additional neural network block and increases the computational complexity of the model. In addition, only the MERL dataset was considered. These limitations require a further investigation in future studies.

Conflict of interests: Authors declare that they do not have conflict of interests, in particular financial, personal, copyright or any other conflicts of a different nature, which could have influenced the research, as well as the results published in this articles

Financing: Research was carried out without financial support

Accessibility data: All data available in digital or graphic form in the main text manuscript

Using artificial intelligence tools: During preparation manuscript used tool GPT-5 of artificial intelligence (AI) for grammatical and stylistic text checks and for the initial estimation of material parameter values. All fragments processed by him were checked and edited by the authors. AI was not used to generate text, formulas, and tables, formation scientific provisions, receipt results or formulation conclusions. Scientific the provisions, results and conclusions are our own, intellectual by the contribution of the authors

REFERENCES

1. Akenine-Möller, T., Haines, E., Hoffman, N., Pesce, A., Iwanicki, M. & Hillaire, S. “Real-Time rendering”, fourth edition. *A K Peters/CRC Press*. 2018, https://www.scopus.com/pages/publications/85148165550. DOI: https://doi.org/10.1201/b22086.

2. Marschner, S. & Shirley, P. “Fundamentals of computer graphics”, fifth edition. *A K Peters/CRC Press*. 2021. DOI: https://doi.org/10.1201/9781003050339.

3. Bishop, C. M. & Bishop, H. “Deep Learning. Foundations and Concepts”. *Springer Cham*. 2024, https://www.scopus.com/pages/publications/85197102011. DOI: https://doi.org/10.1007/978-3-031-45468-4.

4. Goodfellow, I., et al. “Generative adversarial networks”. *Communications of the ACM*. 2020; 63 (11): 139–144, https://www.scopus.com/pages/publications/85094930828.
DOI: https://doi.org/10.1145/3422622.

5. Mildenhall, B., Srinivasan, P. P., Tancik, M., Barron, J. T., Ramamoorthi, R. & Ng, R. “NeRF: representing scenes as neural radiance fields for view synthesis”. *Communications of the ACM*. 2022; 65 (1): 99–106, https://www.scopus.com/pages/publications/85097226104.
DOI: https://doi.org/10.1145/3503250.

6. Tewari, A., et al. “Advances in neural rendering”. *Computer Graphics Forum*. 2022; 41 (2): 703–735, https://www.scopus.com/pages/publications/85113713339. DOI: https://doi.org/10.1111/cgf.14507.

7. Tewari, A., et al. “State of the art on neural rendering”. *Computer Graphics Forum*. 2020; 39 (2): 701–727, https://www.scopus.com/pages/publications/85090397976. DOI: https://doi.org/10.1111/cgf.14022.

8. Sztrajman, A., Rainer, G., Ritschel, T. & Weyrich, T. “Neural BRDF Representation and Importance Sampling”. *Computer Graphics Forum*. 2021; 40 (6): 332–346, https://www.scopus.com/pages/publications/85108804536. DOI: https://doi.org/10.1111/cgf.14335.

9. Gokbudak, F., Sztrajman, A., Zhou, C., Zhong, F., Mantiuk, R. & Oztireli, C. “Hypernetworks for Generalizable BRDF Representation”. In *Computer Vision – ECCV 2024: 18th European Conference*. 2024. p. 73-89, https://www.scopus.com/pages/publications/85208591990. DOI: https://doi.org/10.1007/978-3-031-73116-7_5.

10. Guarnera, D. & Guarnera, G. C. “Virtual material acquisition and representation for computer graphics”. *Springer Cham*. 2018. DOI: https://doi.org/10.1007/978-3-031-02595-2.

11. Guarnera, G. C., Guarnera, D., Ward, G. J., Glencross, M. & Hall, I. “BxDF material acquisition, representation, and rendering for VR and design”. In *SIGGRAPH Asia 2019 Courses - International Conference on Computer Graphics and Interactive Techniques, SA 2019*. 2019, https://www.scopus.com/pages/publications/85076225986. DOI: https://doi.org/10.1145/3355047.3362092.

12. Zhou, Y. “An overview of BRDF models in computer graphics”. *Theoretical and Natural Science*. 2023; 19: 205–210. DOI: https://doi.org/10.54254/2753-8818/19/20230550.

13. Romanyuk, O., Lytvynenko, V. & Zavalniuk, Y. “Modified cosine-quadratic reflectance model”. *Informatyka, Automatyka, Pomiary w Gospodarce I Ochronie Środowiska*. 2025; 15 (1): 45–48, https://www.scopus.com/pages/publications/105002345943. DOI: http://doi.org/10.35784/iapgos.7384.

14. Lafargue-Tallet, T., et al. “Active thermo-reflectometry for absolute temperature measurement by infrared thermography on specular materials”. *Scientific Reports*. 2022; 12: 1–19, https://www.scopus.com/pages/publications/85129962353. DOI: https://doi.org/10.1038/s41598-022-11616-8.

15. Kurt, M. “Real-Time Shading with Phong BRDF Model”. *Dokuz Eylul University Faculty of Engineering Journal of Science and Engineering*. 2019; 21 (63): 859–867. DOI: https://doi.org/10.21205/deufmd.2019216315.

16. Romanyuk, O., Zavalniuk, Y., Romanyuk, O., Snigur, A., Titova, N. & Maidaniuk, V. “The development of physically correct reflectance model based on logarithm function”. In *2023 13th International Conference on Advanced Computer Information Technologies (ACIT)*. 2023. p. 483–487,

https://www.scopus.com/pages/publications/85175545642.
DOI:https://doi.org/10.1109/ACIT58437.2023.10275589.

17. Romanyuk, O., et al. “Optical system visualization of combined reflectance model based on cubic and quadratic functions”. In *Optical Fibers and Their Applications 2023*. 2023, https://www.scopus.com/pages/publications/85197248879. DOI: https://doi.org/10.1117/12.3023138.

18. Romanyuk, O., et al. “New surface reflectance model with the combination of two cubic functions usage”. *Informatyka, Automatyka, Pomiary W Gospodarce I Ochronie Środowiska*. 2023; 13 (3): 101–106, https://www.scopus.com/pages/publications/85173966234.
DOI: https://doi.org/10.35784/iapgos.5327.

19. Ichikawa, T., Fukao, Y., Nobuhara, S. & Nishino, K. “Fresnel microfacet BRDF: Unification of polari-radiometric surface-body reflection”. In *IEEE/CVF Conference on Computer Vision and Pattern Recognition (CVPR)*. 2023. p. 16489–16497, https://www.scopus.com/pages/publications/85173961466. DOI:https://doi.org/10.1109/CVPR52729.2023.01582.

20. Romanyuk, O., Zavalniuk, Y., Romanyuk, O., Kotlyk, S., Bobko, O. & Melnyk, O. “New illumination model for rendering”. In *2025 15th International Conference on Advanced Computer Information Technologies (ACIT)*. 2025. p. 723–727, https://www.scopus.com/pages/publications/105019977938. DOI: https://doi.org/10.1109/ACIT65614.2025.11185657.

21. Hofherr, F., Haefner, B. & Cremers, D. “On neural BRDFs: A thorough comparison of state-of-the-art approaches”. In *2025 IEEE/CVF Winter Conference on Applications of Computer Vision (WACV)*. 2025. p. 1785–1794, https://www.scopus.com/pages/publications/105003635526.
DOI: https://doi.org/10.1109/WACV61041.2025.00181.

22. Volovetskyi, O. “Methods of filtering and regression for forecasting noisy timeseries based on machine learning”. *Herald of Advanced Information Technology*. 2025; 8 (1): 13–27, https://www.scopus.com/pages/publications/105024808646. DOI: https://doi.org/10.15276/hait.08.2025.1.

23. Speranskyy, V. “Accelerating the learning process of a neural network by predicting the weight coefficient”. *Herald of Advanced Information Technology*. 2021; 4 (4): 295–302. DOI: https://doi.org/10.15276/hait.04.2021.1.

24. Tongbuasirilai, T., Unger, J., Guillemot, C. & Miandji, E. “A sparse non-parametric BRDF model”. *ACM Transactions on Graphics (TOG)*. 2022; 41 (5): 181, https://www.scopus.com/pages/publications/85145659907. DOI: https://doi.org/10.1145/3533427.

25. “IOR list”. *Pixel and Poly*. 2022. – Available from: https://pixelandpoly.com/ior.html. –[Accessed: Aug, 2026].

26. “Phong model material properties for some common materials”. *University of Kansas*. 2026. – Available from: https://people.eecs.ku.edu/~jrmiller/Courses/672/InClass/3DLighting/MaterialProperties.html. – [Accessed: Aug, 2026].

27. Filip, J. & Kolafová, M. “Perceptual attributes analysis of real-world materials”. *ACM Transactions on Applied Perception*. 2019; 16 (1): 1–19, https://www.scopus.com/pages/publications/85061215223?. DOI: https://doi.org/10.1145/3301412.

28. Zheng, C., Zheng, R., Wang, R., Zhao, S. & Bao, H. “A compact representation of measured BRDFs using neural processes”. *ACM Transactions on Graphics (TOG)*. 2021; 41 (2): 14, https://www.scopus.com/pages/publications/85126146221. DOI:https://doi.org/10.1145/3490385.

Received 22.07.2024
Received after revision 29,09,2026
Accepted 12.10.2026

DOI: https://doi.org/10.15276/hait.09.2026.33
УДК 004.92

Модифіковані нейронні моделі на основі двопроменевих функцій відбивної здатності

Романюк Олександр Никифорович[1)]
ORCID: https://orcid.org/0000-0002-2245-3364; rom8591@gmail.com. Scopus Author ID: 57105210600
Завальнюк Євген Костянтинович[1)]
ORCID: https://orcid.org/0009-0005-1202-4653; qq9272627@gmail.com. Scopus Author ID: 58643724500

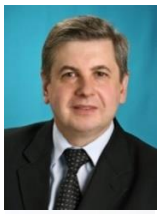
Шевчук Руслан Петрович[2)]
ORCID: https://orcid.org/0000-0001-5381-9528; rulezz.sh@gmail.com. Scopus Author ID: 24178081800
Сиропятов Олександр Арсенійович[3)]
ORCID: https://orcid.org/0000-0002-6362-1280; o.a.syropiatov@op.edu.ua
[1)] Вінницький національний технічний університет, вул. Хмельницьке шосе, 95. Вінниця, 21021, Україна
[2)] Університет в Бельсько-Бялій, Віллова, 2. Бельсько-Бяла, 43-300, Польща
[3)] Національний університет «Одеська політехніка», пр. Шевченка, 1. Одеса, 65044, Україна

АНОТАЦІЯ

Для моделювання відбиття світла від поверхонь об'єктів застосовують двопроменеві функції відбивної здатності. Найбільш часто використовують емпіричні та мікрофасетні аналітичні двопроменеві функції відбивної здатності, що не завжди дозволяють достатньо точно відтворити особливості відбиття світла. Перевагою використання таблиць виміряних значень є високореалістичне подання відбивних властивостей матеріалів. Однак, суттєвим недоліком їх застосування є значні обчислювальні затрати. Для щільного подання таблиць виміряних значень **актуальним** є застосування нейронних двопроменевих функцій відбивної здатності. **Метою дослідження** є розробка модифікованих нейронних моделей, що забезпечують більш продуктивне й точне моделювання відбиття світла від поверхонь матеріалів. У процесі дослідження застосовано **методи** машинного навчання та комп'ютерного моделювання. **Результати дослідження** включають використання фізично значимих характеристик матеріалів разом із єдиним блоком вагових параметрів для компактного подання фіксованого набору матеріалів. Це забезпечує достатньо точне прогнозування значень відбивної здатності без додаткових обчислювальних блоків або перерахунків характеристик матеріалів. Запропоновано також використання нейронних двопроменевих функцій відбивної здатності на основі кластерів матеріалів, що дає можливість використовувати невелику кількість вагових файлів нейромережі та мінімальну кількість характеристик матеріалів, тим самим підвищуючи продуктивність прогнозування значень відбивної здатності. Описано комбінований процес формування кластерів матеріалів. Розглянуто адаптивне комбінування перетворювальних функцій для значень відбивної здатності широкого динамічного діапазону на етапі навчання нейронної моделі. Продемонстровано підвищення точності прогнозування значень відбивної здатності для нових тестових матеріалів. Запропоновані моделі реалізовано у засобі 3D-рендерингу Idx3d. **Висновками** роботи є те, що розроблені моделі дають змогу використовувати єдиний набір вагових параметрів, забезпечують більш продуктивне прогнозування значень відбивної здатності та більш ефективну обробку тренувальних значень.

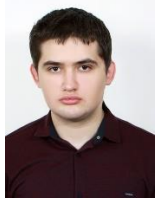
Ключові слова: комп'ютерна графіка; рендеринг; інженерія програмного забезпечення; нейронна мережа; нейронний рендеринг; двопроменева функція відбивної здатності

ABOUT THE AUTHORS



Oleksandr N. Romanyuk - Doctor of Engineering Sciences, Professor, Head of Department of Software Engineering. Vinnytsia National Technical University, 95, Khmelnytske Highway Str. Vinnytsia, 21021, Ukraine
ORCID: https://orcid.org/0000-0002-2245-3364; rom8591@gmail.com. Scopus Author ID: 57105210600
***Research field*:** Computer graphics, formation of graphic images

Романюк Олександр Никифорович - доктор технічних наук, професор, завідувач кафедри Програмного забезпечення. Вінницький національний технічний університет вул. Хмельницьке шосе, 95. Вінниця, 21021, Україна
Галузь досліджень: комп'ютерна графіка, формування графічних зображень



Yevhen K. Zavalniuk - PhD student, Department of Software Engineering. Vinnytsia National Technical University, 95, Khmelnytske Highway Str. Vinnytsia, 21021, Ukraine
ORCID: https://orcid.org/0009-0005-1202-4653; qq9272627@gmail.com. Scopus Author ID: 58643724500
***Research field*:** Computer graphics

Завальнюк Євген Костянтинович - аспірант кафедри Програмного забезпечення. Вінницький національний технічний університет, вул. Хмельницьке шосе, 95. Вінниця, 21021, Україна
Галузь досліджень: комп'ютерна графіка



Ruslan P. Shevchuk - Candidate of Engineering Sciences, Associate Professor, Department of Computer Science and Automatics. University of Bielsko-Biała, 2, Willowa Str. Bielsko-Biała, 43-300, Poland
ORCID: https://orcid.org/0000-0001-5381-9528; rulezz.sh@gmail.com. Scopus Author ID: 24178081800
Research field: Real-time processing of compressed speech signals, development and application of cryptography and steganography methods for protecting speech signals, mobile cyber-physical systems.

Шевчук Руслан Петрович - кандидат технічних наук, доцент кафедри Комп'ютерних наук і автоматизації. Університет в Бельсько-Бялій, Віллова, 2. Бельсько-Бяла, 43-300, Польща
Галузь досліджень: оброблення стиснених мовних сигналів у реальному часі, розробка та застосування методів криптографії та стеганофонії для захисту мовних сигналів, мобільні кібер-фізичні системи



Oleksandr A. Siropiatov - Candidate of Engineering Sciences, Associate Professor, Department of Cybersecurity and Software. Odesa Polytechnic National University. 1, Shevchenko Ave. Odesa, 65044, Ukraine
ORCID: https://orcid.org/0000-0002-6362-1280; o.a.syropiatov@op.edu.ua
***Research field*:** cyberimmune models of data protection

Сиропятов Олександр Арсенійович - кандидат технічних наук, доцент кафедри Кібербезпеки та програмного забезпечення. Національний університет «Одеська політехніка», пр. Шевченка, 1. Одеса, 65044, Україна
Галузь досліджень: кіберімунні моделі захисту даних